FUDMA Journal of Sciences (FJS)
ISSN online: 2616-1370
ISSN print: 2645 - 2944
Vol. 9 No. 2, February, 2025, pp 98 - 104
DOI: https://doi.org/10.33003/fjs-2025-0902-3144

TEMPERATURE VARIATION IN AN A-B BILAYER SYSTEM DURING RADIATION-INDUCED AB COMPOUND LAYER FORMATION

***[1]Akintunde, S. O., [2]Selyshchev, P. A. and [1]Kehinde, D. O.**

[1]Department of Basic Sciences, Babcock University, Ilishan-Remo, Ogun State, Nigeria.
[2]Department of Physics, University of Pretoria, Hatfield Campus, South Africa.

*Corresponding authors' email: akintundes@babcock.edu.ng

ABSTRACT

Metal silicide formation plays a crucial role in microelectronics, particularly in contact and interconnect technologies. Traditional silicide fabrication methods rely on high-temperature annealing, which can lead to undesirable effects such as increased surface roughness and poor electrical contact. An alternative approach is irradiation-assisted silicide formation, which offers advantages such as lower processing temperatures and improved material properties. Understanding the thermal dynamics during irradiation-induced silicide growth is essential for optimizing this process. In this study, we present a mathematical model that describes the temperature dynamics in an A (metal) - B (silicon) bilayer system under the influence of radiation-induced heating during the formation of an AB (metal silicide) compound layer. The model describes heat generation rates within three irradiated A, AB, and B layers, each with distinct material properties. In this work, we used the nickel-silicon bilayer system as a case study. The result from this study shows that the heat generation rate exhibits both linear and parabolic dependencies on layer thickness and temperature change within the nickel silicide layer during radiation-induced heating. Furthermore, the model reveals a significant finding: the temperature obtained in this study for nickel silicide growth under irradiation is lower than its formation temperature under non-irradiation conditions (e.g., conventional heating processes). This result highlights one of the key advantages of employing irradiation techniques over non-irradiation methods. Lastly, the results also show that the thermal vacancy mechanism is not the dominant atomic transport mechanism during the irradiation of the nickel-silicon bilayer system.

Keywords: Heat generation rate, Heat transfer coefficient, Layer thickness, Radiation induced heating, Radiation particle, Temperature change

INTRODUCTION

Experiments have shown the feasibility of compound layer formation, particularly at the interfaces of two immiscible solid layers, when subjected to low-temperature irradiation (Matsuoka et al., 1997; Chakraborty et al., 2005; Agarwal et al., 2010; Arranz, and Palacio, 2009; Tamulevičius et al., 1991; Majni et al., 1982; Jian-Qiang et al., 1989; Boussaa et al., 2005; D'Anna et al., 1986). Much of the prior research in this area was conducted independently using either heavy or light particle beam irradiation. For example, nickel silicide was observed at the interface of a nickel/silicon system under argon ion irradiation (Matsuoka et al., 1997; Boussaa et al., 2005), while cobalt silicide formed at the interface of a cobalt/silicon system under gold ion irradiation (Chakraborty et al., 2005). Additionally, tungsten disilicide was produced at the interface of a tungsten/silicon system under gold ion irradiation, and vanadium disilicide emerged at the interface of a vanadium/silicon system under argon ion irradiation (Arranz, and Palacio, 2009). These specific silicides were also observed under electron and laser irradiation (Majni et al., 1982; Wakita et al., 1983).

These studies reveal that compound layers were primarily formed through a cascade mixing process under heavy particle irradiation, such as ion irradiation. However, this explanation is not directly applicable to light particle irradiation, such as electron irradiation, due to the significant mass difference between electrons and target atoms.

In our study, we propose an alternative approach aimed at explaining compound layer formation from the perspective of radiation-induced processes, which underlie all irradiation techniques. Radiation-induced processes encompass a number of phenomena, all of which occur within a transient time frame during the irradiation period. These processes include radiation-induced heating, radiation-induced defect generation, radiation-induced excitation and ionization, radiation-induced recombination, and annihilation of defects, among others. Due to the various processes at play, it remains unclear which of them is primarily responsible for the formation of compound layers at the interface of an irradiated bilayer system, such as a metal-silicon system.

The radiation-induced processes within the irradiated bilayer systems are considered over a time period much greater than 10^{-8} seconds. During this time frame, defect reactions due to thermal migration are active within the irradiated layers (Was, 2007). The radiation-induced excitation process gradually transforms into heating over this time period. The influence of the radiation-induced ionization process on compound layer formation within this brief interval is negligible, as a vast number of atoms are diffusing almost simultaneously within the irradiated layers. Similarly, the influence of radiation-induced recombination processes can be disregarded over this time frame due to the weak correlation resulting from the spatial separation between vacancies and interstitial atoms within the irradiated systems (Akintunde and Selyshchev, 2016).

Recombination processes occur on a much longer timescale, beyond 10 nanoseconds, compared to the period between 100 femtoseconds and 10 picoseconds, which is characteristic of the displacement cascade phenomenon. As a result, radiation-induced heating and radiation-induced defect generation processes have a more significant impact on the growth of compound layers during times greater than 10^{-8} seconds. These two processes are closely associated with thermal relaxation and diffusion phenomena within the irradiated layer. It is important to note that this investigation focuses on low-temperature conditions, as empirical observations have

shown that most silicides and other intermetallic compounds tend to form at low temperatures (Matsuoka et al., 1997; Chakraborty et al., 2005; Agarwal et al., 2010; Arranz, and Palacio, 2009; Tamulevičius et al., 1991).

This study independently examines the role of radiation-induced heating on atomic diffusion. Specifically, we investigate the temperature associated with heating within each irradiated layer and consider how this temperature facilitates the transport mechanisms of atoms within each irradiated layer toward the reaction interface.

Model and Basic Equations

Suppose that the A and B layers in the A-B bilayer system are irradiated by a low-energy particle beam. The energy transferred by the radiation particles to the target atoms A and B are assumed to be lower than the threshold displacement energies in their respective layers. Consequently, this interaction does not lead to defect generation in the irradiated A and B layers. A substantial portion of the radiation particle energy is converted into heat through their interaction with both layers.

However, it is important to note that the heat intensity in each irradiated layer is not uniform. The energy deposited in these layers varies due generated to differences in particle penetration depths and material composition. Consequently, both the A and B layers heat up as radiation particles deposit energy in them. The thermal vacancies are created and the breaking of atomic bonds within the irradiated layers result from this heating.

In response to this thermal energy, A and B atoms diffuse from their respective layers through thermal vacancies, reaching the reaction interface(s). Here, A-atoms chemically react with B- atoms, forming an AB-compound layer. The bonds formed in the sublattices of the AB- compound layer are distinct from those in the A and B target layers, making the AB compound layer inherently different.

Moreover, the AB-layer also experiences heating due to energy deposition by radiation particles. However, the energy deposited in the AB-layer differs from that in the A and B layers, primarily due to variations in particle penetration depth, which is dimensionally distinct from the A and B layers.

Figure 1 illustrates the geometry of the A-B bilayer system during radiation-induced heating. The thicknesses of the A, AB, and B layers are represented as $h_A(t)$, $h_{AB}(t)$, and $h_B(t)$, with these thicknesses being functions of time t. The temperature increases in the A, AB, and B layers due to radiation-induced heating are denoted as ΔT_A, ΔT_{AB}, and ΔT_B, respectively. T_e, represents the environmental temperature of the A-B bilayer system. Furthermore, T_1, T_2, T_3, and T_4 correspond to temperatures at points X_1, X_2, X_3, and X_4, respectively, with J_1, J_2, J_3, and J_4 representing the respective fluxes at these points.

The heat generation rate, which quantifies the amount of heat energy produced per unit volume per unit time, in the A, AB, and B layers, is represented as Q_A, Q_{AB}, and Q_B respectively

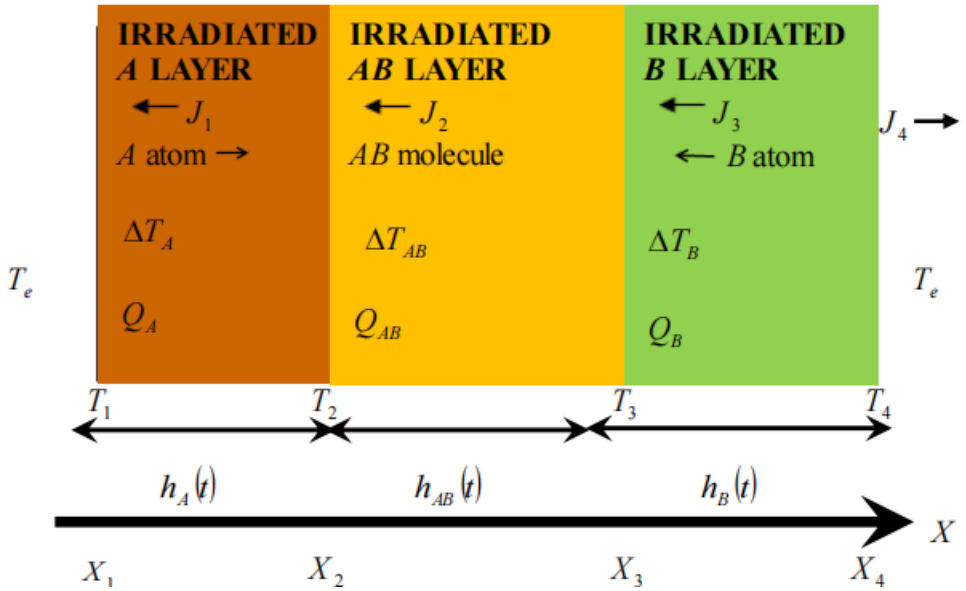

Figure 1: Schematic diagram of the *A-B bilayer* system during radiation induced heating

The equation for the heat distribution in the irradiated layers is described as thus:

$$c\rho\frac{\partial T}{\partial t} + Q = \eta\frac{\partial^2 T}{\partial X^2} \quad (1)$$

With the following boundary conditions:

$$J_1(X_1) = \xi_1(T_e - T_1) \quad (2a)$$

$$J_1(X_2) = J_2(X_2) \quad (2b)$$

$$J_2(X_3) = J_3(X_3) \quad (2c)$$

$$J_4(X_4) = \xi_2(T_4 - T_e) \quad (2d)$$

$$J(X) = -\eta\frac{dT}{dX} \text{ (heat flux equation)} \quad (3)$$

where

ξ_1 is the rate of heat transfer coefficient between the *A* layer and the environment,

ξ_2 is the rate of heat transfer coefficient between the *B* layer and the environment.

c , ρ , and η are the specific heat capacity, density, and thermal conductivity of the irradiated layers respectively.

We assume that $\xi_1 = \xi_2 = \xi$ (for a simple case).

The solution of Eqn. (1) is written as follows under a steady state condition $\left(\text{i.e.}\frac{\partial T}{\partial t} = 0\right)$:

$$T(X) = \frac{Q}{2\eta}(X^2 - X(X_f + X_i) + X_i X_f) + \frac{T_f(X - X_i) + T_i(X_f - X)}{X_f - X_i} \quad (4)$$

The general equation for the temperature of each interface in A-B bilayer system is described by Eqn. (4).

Equation (4) applies to each irradiated layer in the following way:

In the A layer (where i = 1 and f = 2), the temperature of each interface is expressed as:

$$T_A(X) = \frac{Q_A}{2\eta_A}(X^2 - X(X_2 + X_1) + X_1X_2) + \frac{T_2(X - X_1) + T_1(X_2 - X)}{X_2 - X_1} \quad (5)$$

The heat fluxes $J_1(X_1)$ and $J_1(X_2)$ at points X_1 and X_2 along the irradiated A layer are obtained respectively as:

$$J_1(X_1) = -\eta_A\frac{dT_A}{dX} = \frac{Q_A}{2}(X_2 - X_1) - \frac{\eta_A(T_2 - T_1)}{X_2 - X_1} \quad (6)$$

$$J_1(X_2) = -\eta_A\frac{dT_A}{dX} = -\frac{Q_A}{2}(X_2 - X_1) - \frac{\eta_A(T_2 - T_1)}{X_2 - X_1} \quad (7)$$

The temperature of each interface in the AB layer (where i = 2 and f = 3) is given as:

$$T_{AB}(X) = \frac{Q_{AB}}{2\eta_{AB}}(X^2 - X(X_3 + X_2) + X_2X_3) + \frac{T_3(X - X_2) + T_2(X_3 - X)}{X_3 - X_2} \quad (8)$$

The corresponding heat fluxes $J_2(X_2)$ and $J_2(X_3)$ along the irradiated AB layer at points X_2 and X_3 in accordance to Eqn. (3) are derived as:

$$J_2(X_2) = \frac{Q_{AB}}{2}(X_3 - X_2) - \frac{\eta_{AB}(T_3 - T_2)}{X_3 - X_2} \quad (9)$$

$$J_2(X_3) = -\frac{Q_{AB}}{2}(X_3 - X_2) - \frac{\eta_{AB}(T_3 - T_2)}{X_3 - X_2} \quad (10)$$

The temperature of each interface in the B layer (where i = 3 and f = 4) is described by:

$$T_B(X) = \frac{Q_B}{2\eta_B}(X^2 - X(X_4 + X_3) + X_3X_4) + \frac{T_4(X - X_3) + T_3(X_4 - X)}{X_4 - X_3} \quad (11)$$

The heat fluxes $J_3(X_3)$ and $J_4(X_4)$ along the irradiated B layer, in accordance to Eqn. (3), at points X_3 and X_4 are respectively obtained as:

$$J_3(X_3) = \frac{Q_B}{2}(X_4 - X_3) - \frac{\eta_B(T_4 - T_3)}{X_4 - X_3} \quad (12)$$

$$J_4(X_4) = -\frac{Q_B}{2}(X_4 - X_3) - \frac{\eta_B(T_4 - T_3)}{X_4 - X_3} \quad (13)$$

To solve for temperature rise ΔT_A, ΔT_{AB}, and ΔT_B we apply the boundary conditions in
Eqns. (2a) - (2d) to Eqns. (5), (8) and (11).
By replacing $J_1(X_1)$, $J_1(X_2)$, $J_2(X_2)$, $J_2(X_3)$, $J_3(X_3)$ and $J_4(X_4)$ by the expressions in Eqns. (6), (7), (9), (10), (12) and (13) respectively, the boundary conditions in Eqns. (2a) - (2d) become:

$$\xi(T_e - T_1) = \frac{Q_A}{2}(X_2 - X_1) - \frac{\eta_A(T_2 - T_1)}{X_2 - X_1} \quad (14)$$

$$-\frac{Q_A}{2}(X_2 - X_1) - \frac{\eta_A(T_2 - T_1)}{X_2 - X_1} = \frac{Q_{AB}}{2}(X_3 - X_2) - \frac{\eta_{AB}(T_3 - T_2)}{X_3 - X_2} \quad (15)$$

$$-\frac{Q_{AB}}{2}(X_3 - X_2) - \frac{\eta_{AB}(T_3 - T_2)}{X_3 - X_2} = \frac{Q_B}{2}(X_4 - X_3) - \frac{\eta_B(T_4 - T_3)}{X_4 - X_3} \quad (16)$$

$$-\frac{Q_B}{2}(X_4 - X_3) - \frac{\eta_B(T_4 - T_3)}{X_4 - X_3} = \xi(T_4 - T_e) \quad (17)$$

Recall that in Fig. 1
$X_2 - X_1 = h_A$,
$X_3 - X_2 = h_{AB}$,
$X_4 - X_3 = h_B$,
$T_2 - T_1 = \Delta T_A$,
$T_3 - T_2 = \Delta T_{AB}$, and
$T_4 - T_3 = \Delta T_B$.
We rewrite Eqns. (14)-(17) in terms of the symbols of the temperature rise and thickness of the irradiated layers:

$$\xi(T_e - T_1) = \frac{Q_Ah_A}{2} - \frac{\eta_A\Delta T_A}{h_A} \quad (18)$$

$$-\frac{Q_Ah_A}{2} - \frac{\eta_A\Delta T_A}{h_A} = \frac{Q_{AB}h_{AB}}{2} - \frac{\eta_{AB}\Delta T_{AB}}{h_{AB}} \quad (19)$$

$$-\frac{Q_{AB}h_{AB}}{2} - \frac{\eta_{AB}\Delta T_{AB}}{h_{AB}} = \frac{Q_Bh_B}{2} - \frac{\eta_B\Delta T_B}{h_B} \quad (20)$$

$$-\frac{Q_Bh_B}{2} - \frac{\eta_B\Delta T_B}{h_B} = \xi(T_4 - T_e) \quad (21)$$

We solve Eqns. (18)-(21) simultaneously and the following results are obtained for ΔT_A, ΔT_{AB}, and ΔT_B

$$\Delta T_A = \frac{I_1 + I_2}{I_3} \quad (22)$$

where
$I_1 = 2h_Ah_{AB}\eta_{AB}\eta_B[2Q_Ah_A + Q_Bh_B - Q_{AB}h_{AB}]$,
$I_2 = \xi h_Ah_{AB}\left[\left(Q_Ah_{AB}^2\eta_B - Q_Bh_B{}^2\eta_{AB}\right) - Q_Ah_A(h_{AB}\eta_B + h_B\eta_{AB})\right]$, and
$I_3 = 2\eta_{AB}\left[h_{AB}\eta_A(\eta_B + \xi h_B) - \xi h_A\eta_B\left(\frac{h_{AB}^2\eta_A}{h_A\eta_{AB}} + \frac{h_A\eta_{AB}}{\eta_A}\right)\right]$.

$$\Delta T_{AB} = \frac{M_1 + M_2}{M_3} \quad (23)$$

where
$M_1 = h_{AB}\eta_A\eta_{AB}[2h_{AB}\eta_B(Q_Ah_A + Q_Bh_B) - \xi h_Ah_{AB}(Q_{AB}h_{AB} + Q_Bh_B)]$,
$M_2 = h_Ah_{AB}^2[\eta_A\eta_{AB} + 2\xi h_{AB}\eta_B(Q_{AB}\eta_{AB} + Q_A\eta_A) - \xi^2h_{AB}\eta_B(Q_{AB}h_{AB} + Q_Ah_A)]$,
and
$M_3 = 2h_{AB}\eta_{AB}[\eta_A(\eta_{AB}\eta_B + \xi h_B\eta_{AB} - \xi h_{AB}\eta_B) - \xi h_A\eta_{AB}\eta_B]$.

$$\Delta T_B = \frac{V_1[V_2 + V_3(V_4 + V_5)] + V_6}{V_7} \quad (24)$$

where
$V_1 = h_B\eta_A + h_{AB}$,
$V_2 = 2\eta_B[\eta_A + \xi h_B](Q_{AB}h_{AB} + Q_Ah_A)$,
$V_3 = \xi h_{AB}$,
$V_4 = 2\eta_B[3Q_Ah_A + Q_Bh_B - 2Q_{AB}h_{AB}] - \xi h_A(Q_{AB}h_{AB} + Q_Bh_B)$,
$V_5 = (Q_{AB}h_{AB} + Q_Ah_A)\eta_B\left[1 + \xi\left(\frac{h_{AB}}{\eta_{AB}} + \frac{h_A}{\eta_A}\right)\right]$,
$V_6 = \xi h_Ah_{AB}h_B\eta_{AB}[Q_Bh_B(2\eta_B + \xi h_B) + 2\eta_B(Q_{AB}h_{AB} + 2Q_Ah_A) - \xi Q_Ah_Ah_B]$, and
$V_7 = 2h_{AB}\eta_A(2\eta_B + \xi h_B)[\eta_{AB}\eta_B + \xi h_B\eta_{AB} - 2\xi h_{AB}\eta_B]$.
The temperature associated with radiation induced heating is described by:

$$T^{irr} = T_e + \Delta T \quad (25)$$

Two important parameters play a significant role in the calculation of radiation-induced heating: the stopping power of the radiation particle and its depth of penetration in the irradiated layer. For this study, we make the assumption that the depth of penetration of radiation particles in each irradiated layer is equivalent to the layer's thickness. The stopping power of the radiation particle is estimated using the expression provided in Eqn. (26).
It's worth noting that for a compound layer to form at the reaction interface during irradiation, the range of the radiation particle must be greater than or equal to the thickness of the irradiated layer (Attix, 2008). If this condition is not met, no compound layer will form at the reaction site.
In this study, the radiation particle under consideration is an ion. The heat generation rate *'Q'* within each irradiated layer is determined as follows:
At first, we estimate the stopping power for radiation particles in each irradiated layer. The amount of heat energy deposited by the radiation particles during the collision process is calculated as the product of their stopping power and the thickness of the irradiated layer. The quantity *'Q'* is then determined by the product of the defect generation rate, the atomic density of the irradiated layer, the layer thickness, and the stopping power of the radiation particles.
It is worth mentioning that the inclusion of the defect generation rate in the equation describing *'Q'* is to show that the energy intended to create radiation-induced defects is instead transformed into heat energy within the irradiated layers.

The stopping power of the radiation particle in each irradiated layer, according to Ziegler and Biersack (1985), is described by:

$$S_p = \frac{8.462\text{x}10^{-15} A_p Z_t Z_p \theta}{(A_p+A_t)\left(Z_p^{0.23}+Z_t^{0.23}\right)} + \frac{3.83\text{x}10^{-15}\, Z_p^{\frac{7}{6}} Z_t E_k^{0.5}}{A_p^{0.5}\left(Z_p^{\frac{2}{3}}+Z_t^{\frac{2}{3}}\right)^{1.5}} \qquad (26)$$

where

z_t and z_p are the atomic numbers of atoms in the irradiated layer and radiation particles respectively,

A_t and A_p are the corresponding atomic masses of atoms in the irradiated layer and radiation particles.

E_k is the kinetic energy of the radiation particle.

θ is defined by Swalin (1962) as:

$\theta = \frac{\text{Lni}}{\text{i}}$ when i > 30 keV

and

$\theta = \frac{\text{Ln}[1+1.1383\text{i}]}{2(\text{i}+0.01321\text{i}^{0.21226}+0.19593\text{i}^{0.5})}$ when i ≤ 30 keV

where

$$\text{i} = \frac{32.53 A_t E_k}{Z_t Z_p (A_p+A_t)\left(Z_p^{0.23}+Z_t^{0.23}\right)} \qquad (27)$$

The volumetric heat generation rate in the A and B irradiated layers is described by:

$$Q_{A(B)} = S_p h_{A(B)} K n^0_{A(B)} \qquad (28)$$

The volumetric heat generation rate in the AB layer is defined as:

$$Q_{AB} = \upsilon_A Q_A \frac{n_{AB}}{n_A^0} + \upsilon_B Q_B \frac{n_{AB}}{n_B^0} \qquad (29)$$

where υ_A and υ_B are the stoichiometric ratio of A- and B-atoms respectively; n_A^0, n_B^0, and n_{AB} are densities of A, B and AB species in their respective layers; K is the defect generation rate.

RESULTS AND DISCUSSION

The volumetric heat generation rate and the corresponding temperature rise in each irradiated layer are estimated under heavy particle irradiation. The bilayer system under consideration is nickel-silicon system. This bilayer system produced the same kind of silicide as the one described under non-irradiation process in the literature (Bower et al., 1973; Whang et al., 1989; Sisodia et al., 2011).

To determine the temperature rise in the metal layer (A layer), we employ Eqn. (22), and for the silicon layer (B layer), Eqn. (24) is used for the estimation. As for the temperature rise within the silicide layer (AB layer), Eqn. (23) is used. All these estimations are done under the consideration of heavy particle irradiation.

The calculations for heat generation rates in both metal and silicon layers are obtained using Eqn. (28). For the silicide layer under the same irradiation conditions, the heat generation rate is determined with Eqn. (29).

The required data for finding the temperature rise in each layer is presented in Table 1. Tables 2 to 4, contain the estimated values for stopping power, heat generation rate, and temperature rise within each target layer under irradiation.

Table 1: Useful data for the estimation of temperature rise in each irradiated layer in nickel-silicon bilayer system

Layer	E_{exc} (eV)	η(W/m.K)	ρ (kg/m^3)	Z	A	n(10^{28} m^{-3})
Si	171.20	150.00	2330.00	14.00	28.00	5.00
Ni	306.30	91.00	8910.00	28.00	58.70	9.14
Ni_2Si	-	18.20	7890.00	-	145.50	3.30

where E_{exc} is the mean excitation energy and n is the density of atomic species in the irradiated layer.

Table 2: Heat generation rate and temperature rise in nickel layer at a stopping power of 3.71 x 10^{-6} J/m

h_A (10^{-9} m)	Q_A (10^{13} J/m^3.s)	ΔT_A (10^{-6} K)	T_A^{irr} (K)
50	1.69	770.00	298
40	1.35	320.00	298
30	0.92	135.00	298
20	0.68	40.00	298
10	0.13	5.01	298
0	0.00	0.00	298

Table 3: Heat generation rate and temperature rise in silicon layer at a stopping power of 1.45 x 10^{-6} J/m

h_B (10^{-9} m)	Q_B (10^{13} J/m^3.s)	ΔT_B (10^{-6} K)	T_B^{irr} (K)
50	5.63	260.00	298
40	4.22	130.00	298
30	3.66	57.00	298
20	1.45	17.00	298
10	0.23	2.10	298
0	0.00	0.00	298

Table 4: Heat generation rate and temperature rise in nickel silicide layer

h_{AB} (10^{-9} m)	Q_{AB} (10^{13} J/m^3.s)	ΔT_{AB} (10^{-6} K)	T_{AB}^{irr} (K)
0	0.00	0.00	298
10	0.30	2.55	298
20	0.59	268.00	298
30	0.88	690.00	298
40	1.17	1620.00	298
50	1.47	5020.00	298

Prior to the initiation of the irradiation process in the A-B bilayer system, the AB-layer was entirely absent. The irradiation process commences with the A and B layers, and after a short duration, the AB layer begins to form due to a chemical interaction between A-atoms and B-atoms. These atoms diffuse through a vacancy mechanism to the reaction interfaces A/AB and AB/B. As more A and B atoms depart from their respective layers, the thickness of both the A and B layers decreases in dimension. In contrast, the thickness of the AB layer continues to increase dimensionally. This accounts for the observed trend in thickness values as shown in Tables 2 and 3, where the thickness decreases from 50 nm to 0 (zero), while Table 4 shows the opposite trend, with thickness increasing from 0 (zero) to 50 nm. These thickness values were selected arbitrarily; however, they are roughly on the same order of magnitude as those referenced in the literature (Agarwal et al., 2010; Boussaa et al., 2005; Akintunde and Selyshchev, 2016).

The estimated results on heat generation rates and temperature rise of each irradiated layer show that the amount of heat produced per unit volume in unit time during the interaction of argon ion with the atomic species of each layer is not the same as shown in Tables 2 to 4. The reason for the different results shown in these Tables can be attributed to the material properties and composition of the irradiated layers which are different from one layer to another. The material properties of the irradiated layer determine the response of the layer to the radiation heating.

The material properties of nickel, silicon, and nickel silicide are depicted in Table 1. The density and the atomic number of nickel are more than that of silicon. A material with higher atomic number and density is expected to interact strongly with radiation and absorb more of the radiation energy which could lead to higher heating in the material. This explain why the temperature rise in irradiated nickel layer is greater than that in silicon layer when compared the results in Table 2 with those in Table 3 under the same irradiation condition.

A material with lower thermal conductivity would experience higher temperature than the material with higher thermal conductivity because it has lower heat transfer ability, and it can retain more heat leading to higher temperature rise. This also corroborate the results presented in Tables 2 and 3.

The graphs presented in Figs. 2 and 3 reveal a linear (but non uniform) relationship between the heat generation rate and the thickness of both the nickel and silicon layers. Interestingly, Fig. 4 displays an inverse trend for the nickel silicide layer.

These graphical representations offer significant insights into the distribution of heat within these materials. Notably, they suggest that the heat distribution in both the nickel and silicon layers is characterized by non-uniformity, while, in contrast, the nickel silicide layer exhibits a uniform and consistent distribution of heat.

Table 5: The estimation of diffusivities for silicon and nickel during the irradiation process

Irradiated layer	E_v^m (eV)	T^{irr} (K)	D_v^{irr} (m²/s)	D_{th}^{irr} (m²/s)	a (10^{-10} m)
Si	[a]1.06	298	[a]1.50 x 10^{-16}	1.72 x 10^{-49}	5.40
Ni	[b]1.04	298	[a]2.80 x 10^{-20}	1.60 x 10^{-49}	3.52

a is obtained from the work of Akintunde and Selyshchev (2016) and b is from the work of Pfeiler (2007)

where E_v^m is the vacancy migration energy, D_v^{irr} is the diffusivity of atoms via radiation induced vacancy mechanism, a is the lattice constant, and D_{th}^{irr} is the diffusivity of atoms via thermal vacancy mechanism.

D_{th}^{irr} in Table 5 is estimated based on the Arrhenius equation of the form:

$$D_{th}^{irr} = a^2 f_v exp\left[\frac{-E_v^m}{kT^{irr}}\right] \quad (30)$$

where

f_v (5 x 10^{-13} s^{-1} (Whang et al., 1989)) is the jump frequency factor for vacancy and k is the Boltzmann constant (8.617 x 10^{-5} eV/K).

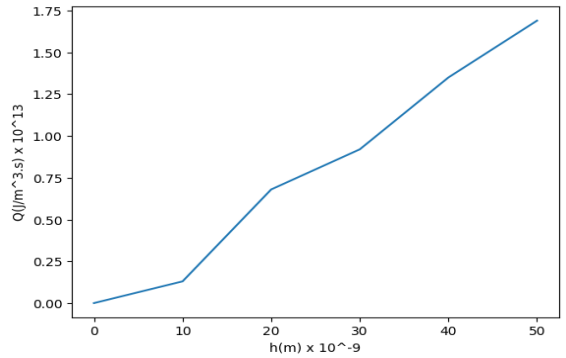

Figure 2: Heat generation rate as a function of thickness in nickel layer

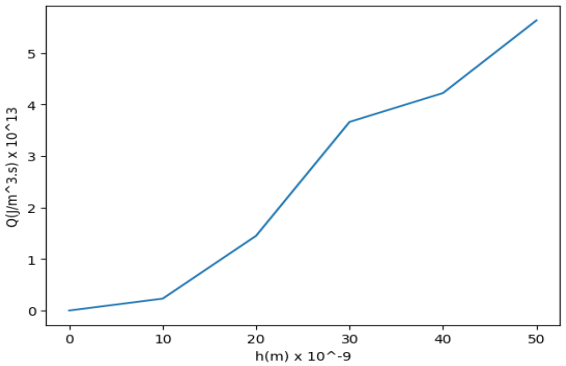

Figure 3: Heat generation rate as a function of thickness in the silicon layer

Figs. 5, 6, and 7 reveal a relationship that illustrates the parabolic dependency of the heat generation rate on temperature variations within the irradiated layers.

The Irradiation temperature T^{irr} of nickel silicide in this work is obtained by substituting the values of temperature rise in Table 4 into Eqn. (25). These results are in good agreement with the experimental work of Boussaa et al. (2005). Experimentally, as demonstrated by Boussaa et al., it was found that nickel silicide forms at room temperature under irradiation. The temperature obtained for each layer, in this work, is the same due to the extremely small temperature rise in each irradiated layer as shown in Tables 2 to 4. The low temperature during the irradiation of metal silicide is one of the reasons why irradiation technique is preferred over conventional heating method because silicides that are formed under irradiation have better electrical properties and smoother surfaces than those formed under non-irradiation techniques (Agarwal et al., 2010).

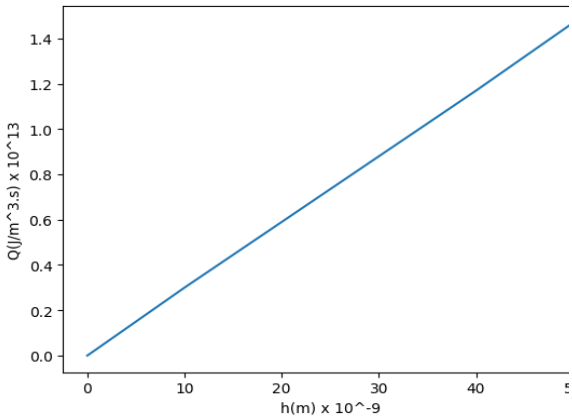

Figure 4: Heat generation rate as a function of thickness in nickel silicide layer

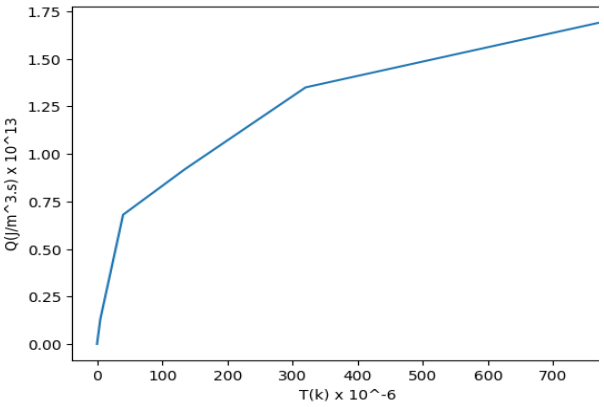

Figure 5: Heat generation rate as a parabolic function of change in temperature in nickel layer

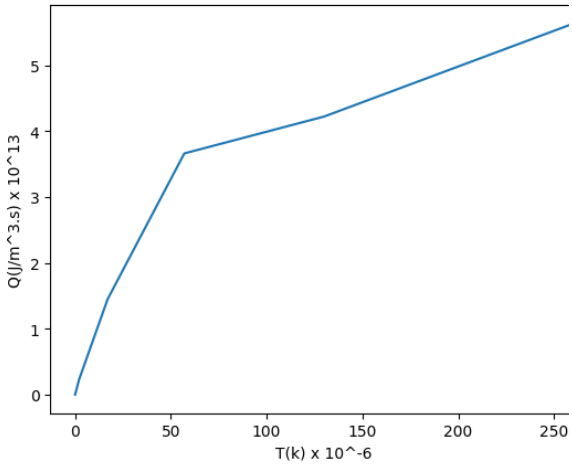

Figure 6: Heat generation rate as a function of temperature change in silicon layer

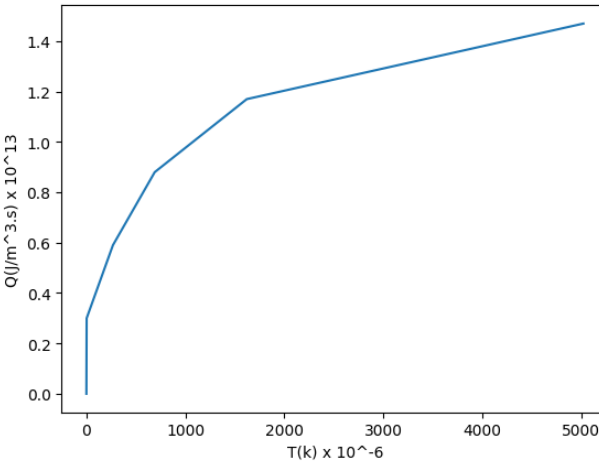

Figure 7: Heat generation rate as a function of temperature change in nickel silicide layer

The results in Table 5 highlight a notable disparity: the irradiation temperature, as determined in this study, appears inadequate to explain the diffusivity of atomic species falling within the order of magnitude that range between 10^{-16} and 10^{-20} m^2/s, as previously reported by Murarka (2012).

It's worth noting that this range of diffusivity is crucial, representing the interdiffusion coefficients required for the growth of silicide layers at the interfaces of metal-silicon systems.

Remarkably, the result from our prior research, in the literature (Akintunde and Selyshchev, 2016), aligns remarkably well with the diffusivity range mentioned in the work reported by Murarka (2012). This congruence suggests a significant implication: during the irradiation process, atomic species within each irradiated layer exhibit substantial diffusion through radiation-induced vacancies, as opposed to thermal vacancies, as they move to the reaction interface, where the formation of metal silicide primarily occurs.

Based on the results reported here, one can conclude that the thermal vacancy mechanism is not the dominant atomic transport mechanism during the irradiation of the nickel-silicon bilayer system.

An intriguing point of comparison emerges when considering the temperature at which nickel silicide forms under non-irradiation conditions, as observed in experimental work, which stands at 473 K (Murarka, 2012). This temperature surpasses the value obtained in our current study.

CONCLUSION

In this study, we have developed a mathematical model that explain the distribution of heat and the corresponding temperature rise within irradiated layers, using the nickel-silicon bilayer system as a case study. Our investigation reveals that the temperature increase in each irradiated layer is not uniform, primarily due to the distinct material properties of these layers. This disparity in temperature rise can be attributed to the different heat generation rates observed in the irradiated layers. This difference arises from the distinct responses of materials to heating under irradiation, a response which is as a result of the unique properties inherent in each irradiated material. Notably, our results indicate a significant finding: a linear relationship exists between the heat generation rate of a nickel silicide layer and its thickness. This suggest that heat is uniformly distributed in nickel silicide layer during irradiation. Furthermore, we establish that the irradiation temperature required for silicide formation is lower than that of the conventional heating methods. This is one of the key reasons for the preference of irradiation techniques over non-irradiation methods.

In practical terms, the silicides produced through irradiation techniques exhibit superior electrical properties and smoother surface characteristics when compared to those formed through conventional heating processes. The results also show that the thermal vacancy mechanism is not the dominant atomic transport mechanism during the irradiation of the nickel-silicon bilayer system.

REFERENCES

Agarwal, G., Kulshrestha, V., Sharma, P., & Jain, I. P. (2010). Change in the microstructure at W/Si interface and surface by swift heavy ions. *Journal of colloid and interface science*, *351*(2), 570-575. https://doi.org/10.1016/j.jcis.2010.07.055

Akintunde, S. O., & Selyshchev, P. A. (2016). The influence of radiation-induced vacancy on The formation of thin-film of compound layer during a reactive diffusion process. *Journal of Physics and Chemistry of Solids*, *92*, 64-69. https://doi.org/10.1016/j.jpcs.2016.01.020

Arranz, A., & Palacio, C. (2009). Low-energy Ar+ ion-beam induced vanadium silicide formation at V/Si interfaces. *Thin Solid Films*, *517*(8), 2656-2660. https://doi.org/10.1016/j.tsf.2008.10.052

Attix, F. H. (2008). *Introduction to radiological physics and radiation dosimetry*. John Wiley & Sons. ISBN 9783527617142

Boussaa, N., Guittoum, A., & Tobbeche, S. (2005). Formation of Ni2Si silicide in Ni/Si bilayers by ion beam mixing. *Vacuum*, *77*(2), 125-130. https://doi.org/10.1016/j.vacuum.2004.07.081

Bower, R. W., Sigurd, D., & Scott, R. E. (1973). Formation kinetics and structure of Pd2Si films on Si. *Solid-State Electronics*, *16*(12), 1461-1471. https://doi.org/10.1016/0038-1101(73)90063-4

Chakraborty, B. R., Halder, S. K., Karar, N., Kabiraj, D., & Avasthi, D. K. (2005). Formation of cobalt silicides as a buried layer in silicon using high energy heavy ion irradiation. *Journal of Physics D: Applied Physics*, *38*(16), 2836. https://doi.org/10.1088/0022-3727/38/16/015

D'Anna, E., Leggieri, G., Luches, A., & Majni, G. (1986). Chromium silicide formation with multiple electron beam pulses. *Thin Solid Films*, *140*(1), 163-166. https://doi.org/10.1016/0040-6090(86)90170-7

Jian-Qiang, L., Zhong-Lie, W., Xun-Liang, D., Ren-Yuan, H., & Fu-Zhai, C. (1989). A study of the chemical driving force in ion mixing of metal-metal systems. *Vacuum*, *39*(2-4), 275-277. https://doi.org/10.1016/0042-207X(89)90217-0

Majni, G., Nava, F., Ottaviani, G., Luches, A., Nassisi, V., & Celotti, G. (1982). Electron beam induced reactions in metal/Si systems. *Vacuum*, *32*(1), 11-18. https://doi.org/10.1016/S0042-207X(82)80189-9

Matsuoka, M., Chubaci, J. F. D., Biersack, J. P., Watanabe, S., Kuratani, N., & Ogata, K. (1997). Nickel metallization of Si by dynamic ion-beam mixing. *Radiation effects and defects in solids*, *143*(1), 65-74. https://doi.org/10.1080/10420159708212949

Murarka, S. P. (2012). *Silicides for VLSI applications*. Academic press. ISBN 9780080570563

Pfeiler, W. (Ed.). (2007). *Alloy physics: a comprehensive reference*. John Wiley & Sons. ISBN 9783527313211

Sisodia, V., Sapnar, K. B., & Dhole, S. (2011). Ti silicide formation by interfacial mixing using swift heavy ion irradiation. *Archives of Physics Research*, *2*(1), 54-67. (http://scholarsresearchlibrary.com/archive.html)

Swalin, R. (1962). Diffusion of interstitial impurities in germanium and silicon. *Journal of Physics and Chemistry of Solids*, *23*(1-2), 154-156. https://doi.org/10.1016/0022-3697(62)90069-0

Tamulevičius, S., Pranevicius, L., & Budinavičius, J. (1991). Application of dynamic ion mixing in platinum silicide formation. *Applied surface science*, *53*, 159-164. https://doi.org/10.1016/0169-4332(91)90257-K

Wakita, A. S., Sigmon, T. W., & Gibbons, J. F. (1983). Oxidation kinetics of laser formed MoSi2 on polycrystalline silicon. *Journal of Applied Physics*, *54*(5), 2711-2715. https://doi.org/10.1063/1.332296

Was, G. S. (2007). *Fundamentals of Radiation Materials Science: Metals and Alloys*. Springer. https://doi.org/10.1007/978-1-4939-3438-6

Whang, C. N., Kim, H. K., Lee, R. Y., & Smith, R. J. (1989). Ar+ ion beam induced silicide formation mechanism at the Pd-Si interface. *Journal of materials science*, *24*, 265-270. https://doi.org/10.1007/BF00660965

Ziegler, J. F., & Biersack, J. P. (1985). The stopping and range of ions in matter. In *Treatise on heavy-ion science: volume 6: astrophysics, chemistry, and condensed matter* (pp. 93-129). Boston, MA: Springer US. https://doi.org/10.1007/978-1-4615-8103-1_3